

Electronic Supplementary Information for

Effect of Organic Ligands in Iron-Based Metal–Organic Frameworks on  
Oxygen Evolution Electrocatalysis: Conventional Inorganic Solids vs.  
Organic–Inorganic Hybrid Materials

Yuuki Sugawara,<sup>a</sup> Kanta Magofuku<sup>a</sup> and Takeo Yamaguchi<sup>\*a</sup>

<sup>a</sup>Laboratory for Chemistry and Life Science, Institute of Integrated Research, Institute of Science  
Tokyo, Yokohama, Kanagawa 226-8501, Japan.

\* Corresponding authors; E-mail: [yamag@res.titech.ac.jp](mailto:yamag@res.titech.ac.jp)

## Methods

### Chemicals

Iron chloride hexahydrate ( $\text{FeCl}_3 \cdot 6\text{H}_2\text{O}$ , 99%), terephthalic acid (95%), sodium hydroxide (NaOH, 93%) and potassium hydroxide (KOH, 85%) were purchased from FUJIFILM Wako Pure Chemical Corporation (Osaka, Japan). 2-Aminobenzene-1,4-dicarboxylic acid (99%), 2,6-naphthalenedicarboxylic acid (99%) and 5 wt% Nafion® solution (product number: 274704) were purchased from Sigma-Aldrich Japan K.K. (Tokyo, Japan), and its cation was exchanged by the addition of 0.1 M KOH aqueous solution. All other chemicals were purchased from FUJIFILM Wako Pure Chemical Corporation and used as received.

### Catalyst Synthesis

*MIL-53-lt*, *MIL-88B*, *MOF-235*, and *NH<sub>2</sub>-MIL-88B* were synthesized via solvothermal methods.<sup>1-4</sup> *MIL-53-lt* was synthesized by dissolving  $\text{FeCl}_3 \cdot 6\text{H}_2\text{O}$  (10 mmol) and terephthalic acid (10 mmol) in anhydrous *N,N*-dimethylformamide (DMF) (50 mL). The solution was transferred into a Teflon-lined autoclave, heated to 150 °C and kept for 65 h. Then, precipitates were collected by centrifugation and washed using DMF, MeOH and water, in this order. The residual solid was dried in vacuo at 70 °C to yield *MIL-53-lt*. *MOF-235* was synthesized by changing the feed ratio of the Fe resource and terephthalic acid.  $\text{FeCl}_3 \cdot 6\text{H}_2\text{O}$  (0.738 mmol) was dissolved in anhydrous EtOH. Terephthalic acid (1.23 mmol) was dissolved in anhydrous DMF (30 mL), and the  $\text{FeCl}_3$  solution was added to this solution

with stirring. The mixture was transferred into a Teflon-lined autoclave, heated to 80 °C and kept for 48 h. Afterward, precipitates were collected by centrifugation and washed using DMF, DMF/EtOH (50/50) and EtOH, in this order. The residual solid was dried in the air to yield MOF-235. MIL-88B was synthesized by modifying the abovementioned protocol. FeCl<sub>3</sub>·6H<sub>2</sub>O (3 mmol) and terephthalic acid (6 mmol) were dissolved in anhydrous DMF (30 mL). Thereafter, 2 M NaOH (2.4 mL) was slowly added to this solution dropwise with stirring. Subsequently, the stirring was continued for 30 min, and the solution was transferred into a Teflon-lined autoclave, heated to 100 °C and kept for 20 h. Afterward, precipitates were collected by centrifugation and washed using DMF and MeOH, in this order. The residual solid was dried in air to yield MIL-88B. NH<sub>2</sub>-MIL-88B was synthesized by replacing terephthalic acid with 2-aminobenzene-1,4-dicarboxylic acid. FeCl<sub>3</sub>·6H<sub>2</sub>O (1 mmol) and 2-aminobenzene-1,4-dicarboxylic acid (1 mmol) were dissolved in anhydrous DMF (20 mL) and stirred for 1 h. The solution was transferred into a Teflon-lined autoclave, heated to 150 °C and kept for 72 h. Afterward, precipitates were collected by centrifugation and washed using MeOH three times and water three times, in this order. The residual solid was dried in vacuo at 50 °C to yield NH<sub>2</sub>-MIL-88B.

MIL-88C was synthesized *via* the precipitation method.<sup>5</sup> Briefly, FeCl<sub>3</sub>·6H<sub>2</sub>O (4.76 mmol) and naphthalene-2,6-dicarboxylic acid (3.42 mmol) were dissolved in anhydrous DMF (50 mL) in a round-bottom flask. The solution was reacted at 130 °C for 18 h with stirring. Thereafter, precipitates were collected by centrifugation and washed with DMF, water and EtOH, in this order. The residual solid was dried in vacuo at room temperature to yield MIL-88C.

## **Material Characterizations**

*X-ray diffraction (XRD)* patterns were collected using a MiniFlex600 (Rigaku Corporation, Akishima, Japan).

*Fourier transform infrared (FTIR)* spectra were recorded on an FTIR spectrometer (FT/IR-6200, JASCO Corp., Hachioji, Japan) at  $4\text{ cm}^{-1}$  resolution.

*Raman* spectroscopy was performed using a confocal Raman microscope (LabRAM HR Evolution, HORIBA Ltd., Kyoto, Japan) equipped with a micro-Raman spectrometer (Renishaw InVia) in the backscattering geometry using a 532 nm excitation laser. The spectra were recorded with a resolution of  $0.2\text{ cm}^{-1}$  using a  $600\text{ gr mm}^{-1}$  grating at ambient temperature.

*Scanning electron microscopy* images were obtained using a Hitachi S-4800 (Hitachi High-Technologies Corporation, Tokyo, Japan) at an accelerating voltage of 5.0 kV.

*Transmission electron microscopy* images were obtained using a Hitachi H-8100 or H-9500 (Hitachi High-Technologies Corporation) at an accelerating voltage of 200 kV.

*Brunauer–Emmett–Teller* surface area analysis with  $\text{N}_2$  adsorbents was carried out using BELSORP-MINI X (MicrotracBEL Corp., Osaka, Japan).

*Thermogravimetry analysis* was performed using a Pyris 1 TGA (PerkinElmer U.S. LLC, Shelton, CT, USA).

*X-ray photoelectron spectroscopy (XPS)* was carried out with a PHI 5000 VersaProbe III instrument

(ULVAC-PHI, Inc., Chigasaki, Japan) using monochromatized Al K $\alpha$  radiation (1486.6 eV). The binding energies were calibrated using the C 1s band energy of 284.8 eV.

## Electrochemical Measurements

The oxygen evolution reaction (OER) activities of catalysts were evaluated on a potentiostat HZ-7000 (MEIDEN HOKUTO CORPORATION, Tokyo, Japan). Hg/HgO (1 M KOH; BAS Inc., Tokyo, Japan) and Pt plate (MICLAB Ltd., Yamato, Japan) were used as reference and counter electrodes, respectively. The potential on the Hg/HgO electrode was converted into the reversible hydrogen electrode (RHE). Hg/HgO was calibrated as reported by Li *et al.*<sup>6</sup> and using the following equation:

$$E_{\text{RHE}} = E_{\text{Hg/HgO}} + 0.9047 \text{ V} \quad (1)$$

The catalyst slurry was fabricated by mixing 0.25 mg of MOF catalyst, 2.25 mg of acid-treated carbon nanotubes (CNTs), 2 mL of isopropyl alcohol, 1 mL of EtOH, and 0.2 mL of 3.3 wt% K $^{+}$  ion-exchanged Nafion®, followed by homogenizing for 10 min and sonicating for 1 h. The resulting slurry was dropped onto both sides of a glassy carbon (GC) plate (038024 Glassy carbon plate, 1 mm thick, type 1, Alfa Aesar, Ward Hill, MA, USA) to fix its loading amount of 20  $\mu\text{L cm}^{-2}$ , and it was dried in air.

The sample catalyst electrodes were pretreated by five cyclic voltammetry (CV) scans between -0.05 and 1.0 V vs. RHE at a scan rate of 50 mV s $^{-1}$  without disk rotation. The OER activities of the catalysts were tested by the CV scan sweeps between 1.2 and 1.8 V vs. RHE at a scan rate of 10

$\text{mV s}^{-1}$  in  $\text{N}_2$ -saturated 1 M KOH at ambient temperature. Reaction currents were calculated by taking the average of the forward and backward sweeps of the 10th cycle to cancel the capacitive currents. Ohmic losses were corrected by the following equation using the measured current ( $i$ ) and electrolyte resistance ( $R$ ), which was determined by alternating current impedance:

$$iR\text{-corrected } E = E_{\text{RHE}} - iR \quad (2)$$

## Theoretical Calculations

Density functional theory (DFT) calculations were executed using the Vienna Ab initio Simulation Package (VASP 6.1.0)<sup>7-10</sup> implemented in the TSUBAME4.0 supercomputer at Institute of Science Tokyo. In the DFT calculations, electronic exchange-correlation interactions were included using the generalized gradient approximation method with a Perdew–Burke–Ernzerhof functional (GGA-PBE).<sup>11</sup> For the on-site Coulombic interactions on the d electrons of Ni, the GGA + U method was applied with the Hubbard U parameter of 4.0 eV. The U value was chosen according to the literature.<sup>12</sup> Spin polarization was allowed in all calculations. An energy cutoff was set to 520 eV, and projector augmented wave pseudopotentials were used for all elements. Convergence thresholds for electronic state calculation and geometrical optimization were set to  $1.0 \times 10^{-6}$  eV and  $2.0 \times 10^{-2}$  eV  $\text{\AA}^{-1}$  in energy and force, respectively. The unit cells and atomic positions of the calculated metal sulfides were optimized. The initial structures of the compounds were collected as crystallographic information files (CIF) format from the Cambridge Crystallographic Data Centre (CCDC). These CIFs were modified

to construct structural models for DFT calculations. Adsorbed water molecules were not considered and were omitted from the crystal structures. Similarly, adsorbed methanol, acetic acid and bromide ions were not considered for MIL-88C and NH<sub>2</sub>-MIL-88B. The calculations for MOF-235 and  $\gamma$ -Fe<sub>2</sub>O<sub>3</sub> were omitted because the former structure contained DMF as an organic ligand, which indicated atomic partial occupancies of its methyl group, and the latter structure contained partial Fe defects at the FeO<sub>6</sub> octahedral sites. Consequently, the atomic positions in their unit cells cannot be defined uniquely. The dimensions of the unit cells are summarized in Table S1. The Monkhorst–Pack scheme k-point grid sampling for the Brillouin zone was adjusted to maintain a k-point spacing of approx. 0.025 Å<sup>-1</sup> in each direction, as shown in Table S1. After geometrical optimization, O *p*- and Fe *d*-band centers were extracted from the projected density of states (PDOS).

The molecular orbital calculations for the organic ligands were carried out based on Hartree–Fock method using the Gaussian16 package program<sup>13</sup> with the 6-31G++(d,p) basis set with geometry optimization. The SMD<sup>14</sup> polarizable continuum solvation model was employed to reflect the solvent effect of water. After the calculations, oxygen 2p orbitals were extracted to determine their energy levels and charge distributions.

## Material characterizations

The XRD patterns presented in Fig. S1–S5 correspond to those of MIL-88B, MOF-235, MIL-53-lt, NH<sub>2</sub>-MIL-88B and MIL-88C, respectively, reported in the Cambridge Crystallographic Data Centre (CCDC) and literature. The crystallite diameters ( $d_{\text{XRD}}$ ) were calculated using the Scherrer equation. The FTIR spectrum of NH<sub>2</sub>-MIL-88B (Fig. S6) is consistent with the previous literature<sup>15</sup> and highlights the presence of amino group. According to the thermogravimetric analysis, each MOF has an iron content close to the corresponding theoretical value, as presented in Fig. 2a. The scanning electron microscopy (SEM) and transmission electron microscopy (TEM) images of each MOF (Fig. 2bc) exhibit needle-like or elongated dipyramidal morphology. Furthermore, the Brunauer–Emmett–Teller specific surface areas ( $S_{\text{BET}}$ ) of these MOFs range from 6 to 23 m<sup>2</sup> g<sup>-1</sup>, and the trends are almost consistent with their  $d_{\text{XRD}}$  values.

## Supplementary figures and tables

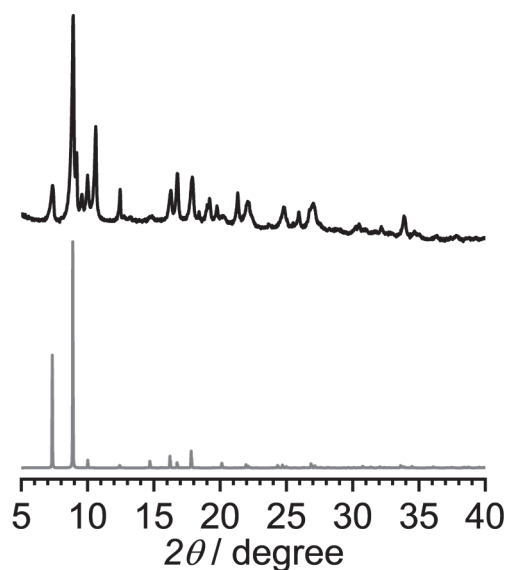


Fig. S1 Measured (upper) and theoretical (lower, CCDC: 2088535) MIL-88B XRD patterns.

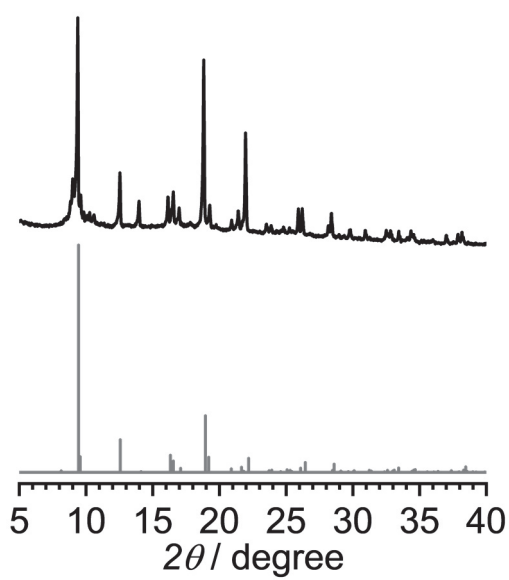


Fig. S2 Measured (upper) and theoretical (lower, Ref. 16) MOF-235 XRD patterns.

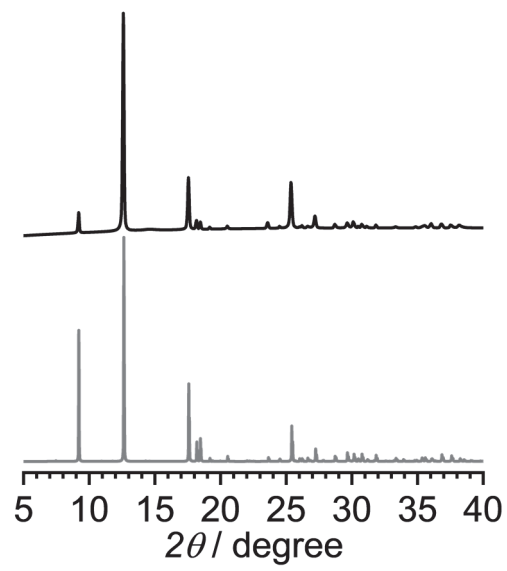


Fig. S3 Measured (upper) and theoretical (lower, CCDC: 690316) MIL-53-lt XRD patterns.

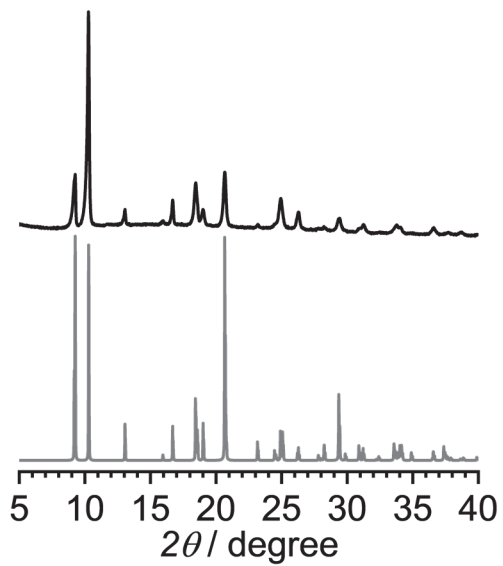


Fig. S4 Measured (upper) and theoretical (lower, CCDC: 647646) NH<sub>2</sub>-MIL-88B XRD patterns.

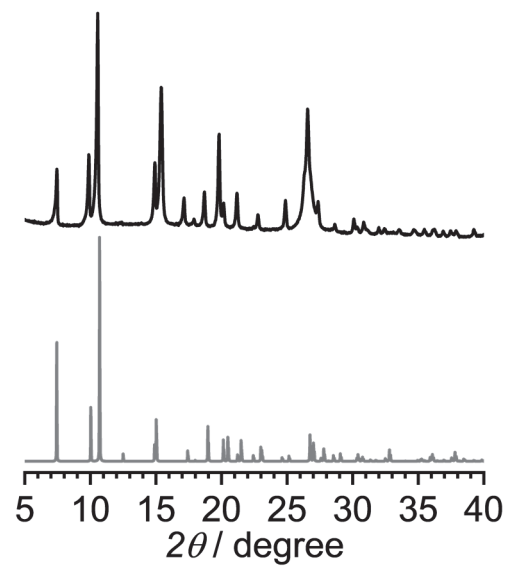


Fig. S5 Measured (upper) and theoretical (lower, CCDC: 285812) MIL-88C XRD patterns.

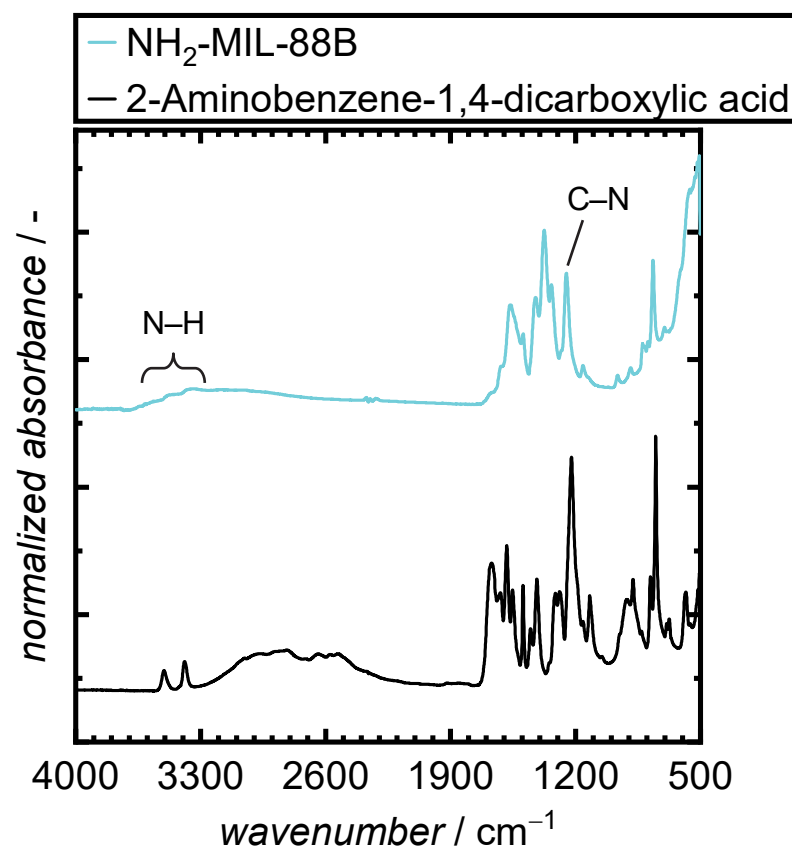


Fig. S6. FTIR spectrum of  $\text{NH}_2\text{-MIL-88B}$  and 2-aminobenzene-1,4-dicarboxylic acid.

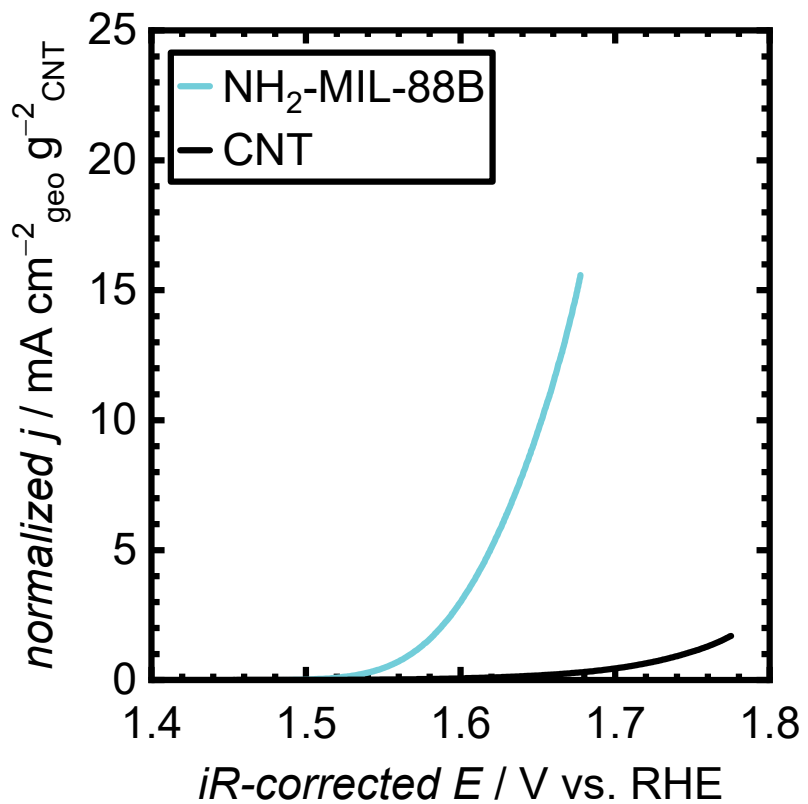


Fig. S7 Comparison of the generated current with CNT electrode in 1 M KOH.

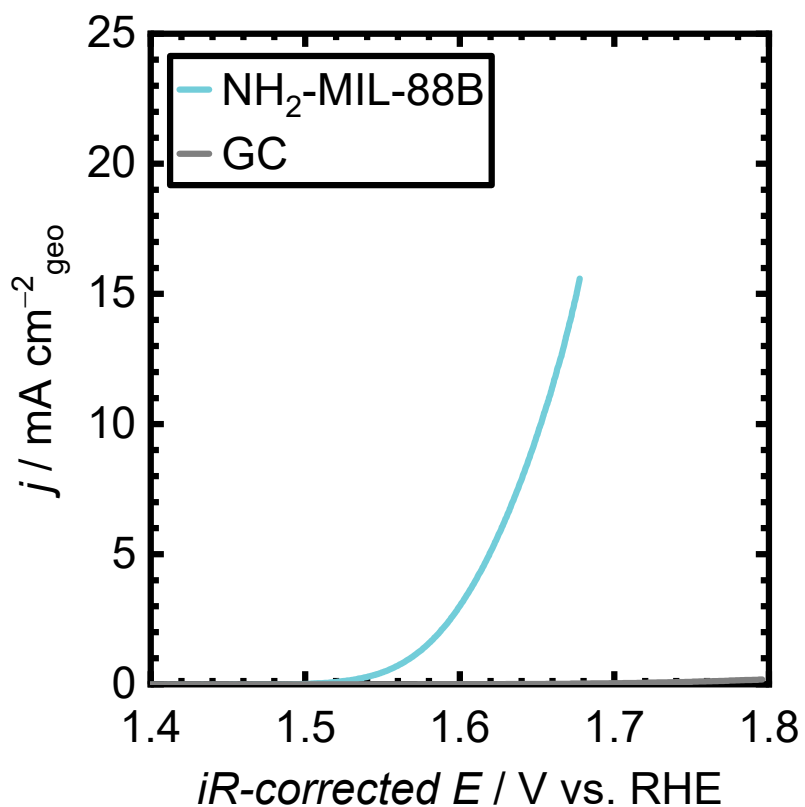


Fig. S8 Comparison of the generated current with a bare glassy carbon electrode in 1 M KOH.

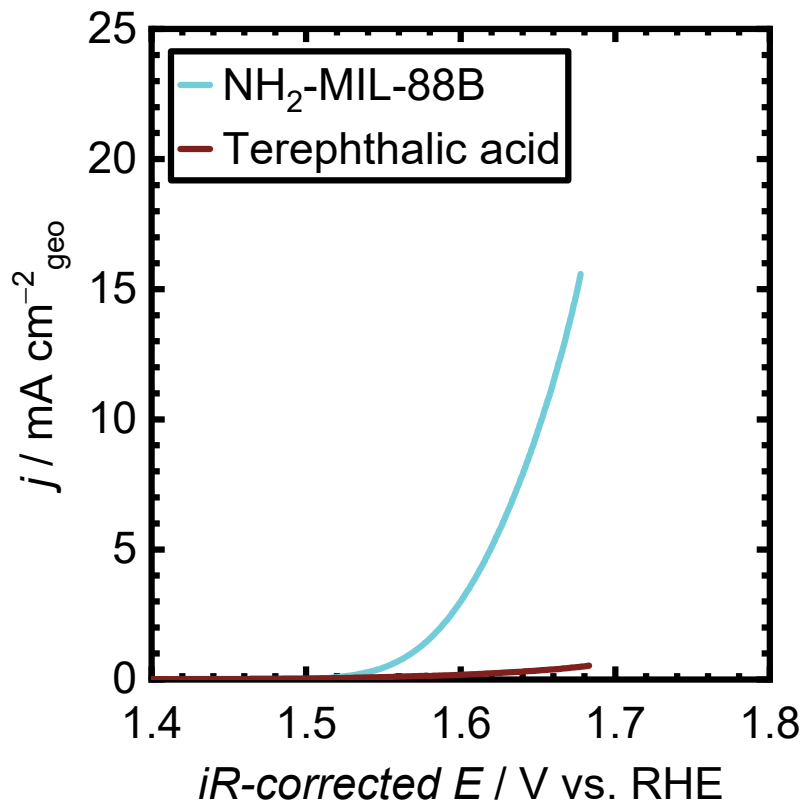


Fig. S9 Comparison of the generated current with an electrode of the terephthalic acid ligand only in 1 M KOH.

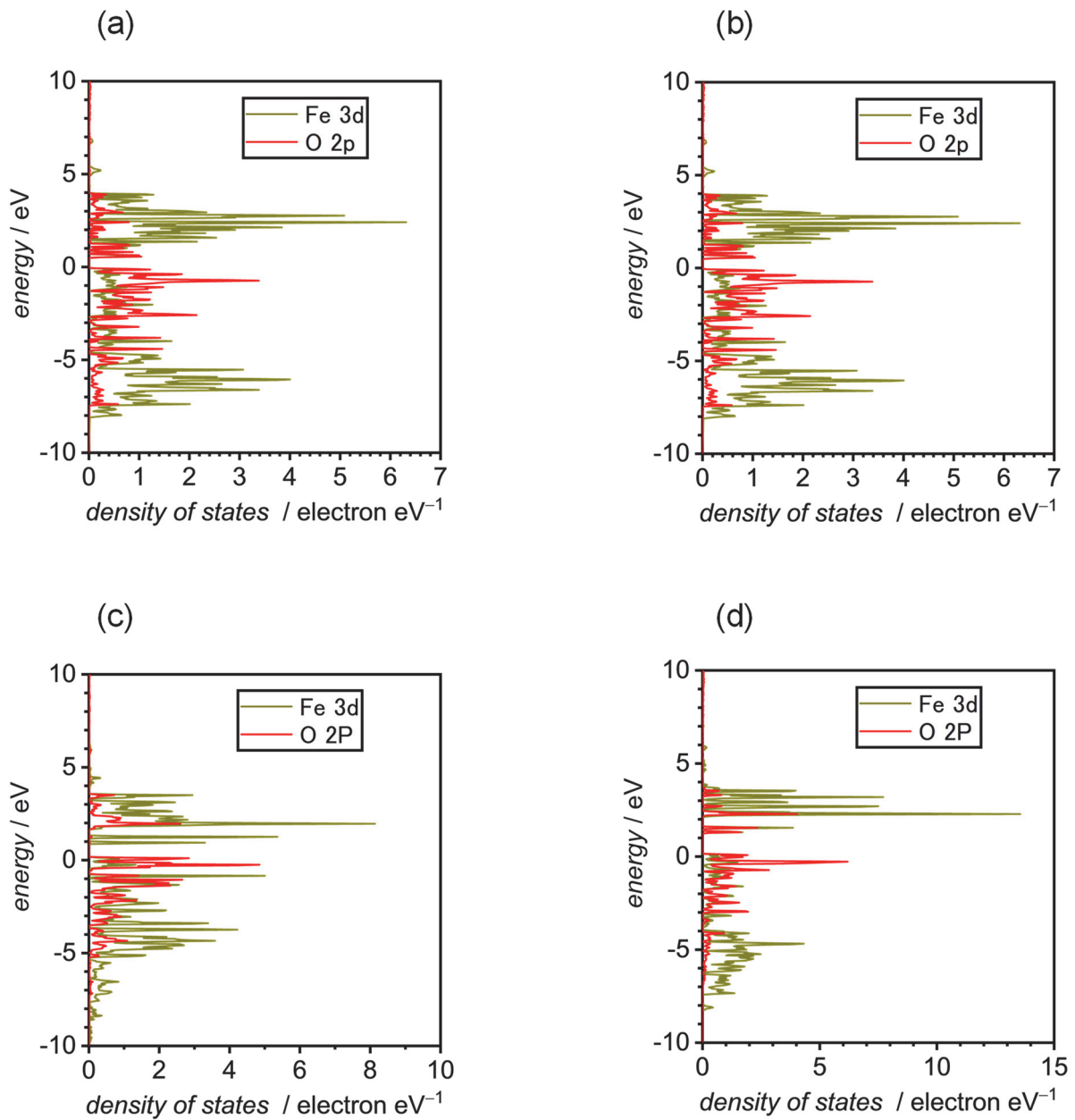


Fig. S10 DFT-calculated PDOS of the O 2p band and Fe 3d band for the exact O and Fe atoms, respectively, which are the components of the minimum Fe–O bond length in each unit cell of (a) MIL-88B, (b) MIL-53-lt, (c) NH<sub>2</sub>-MIL-88B and (d) MIL-88C.

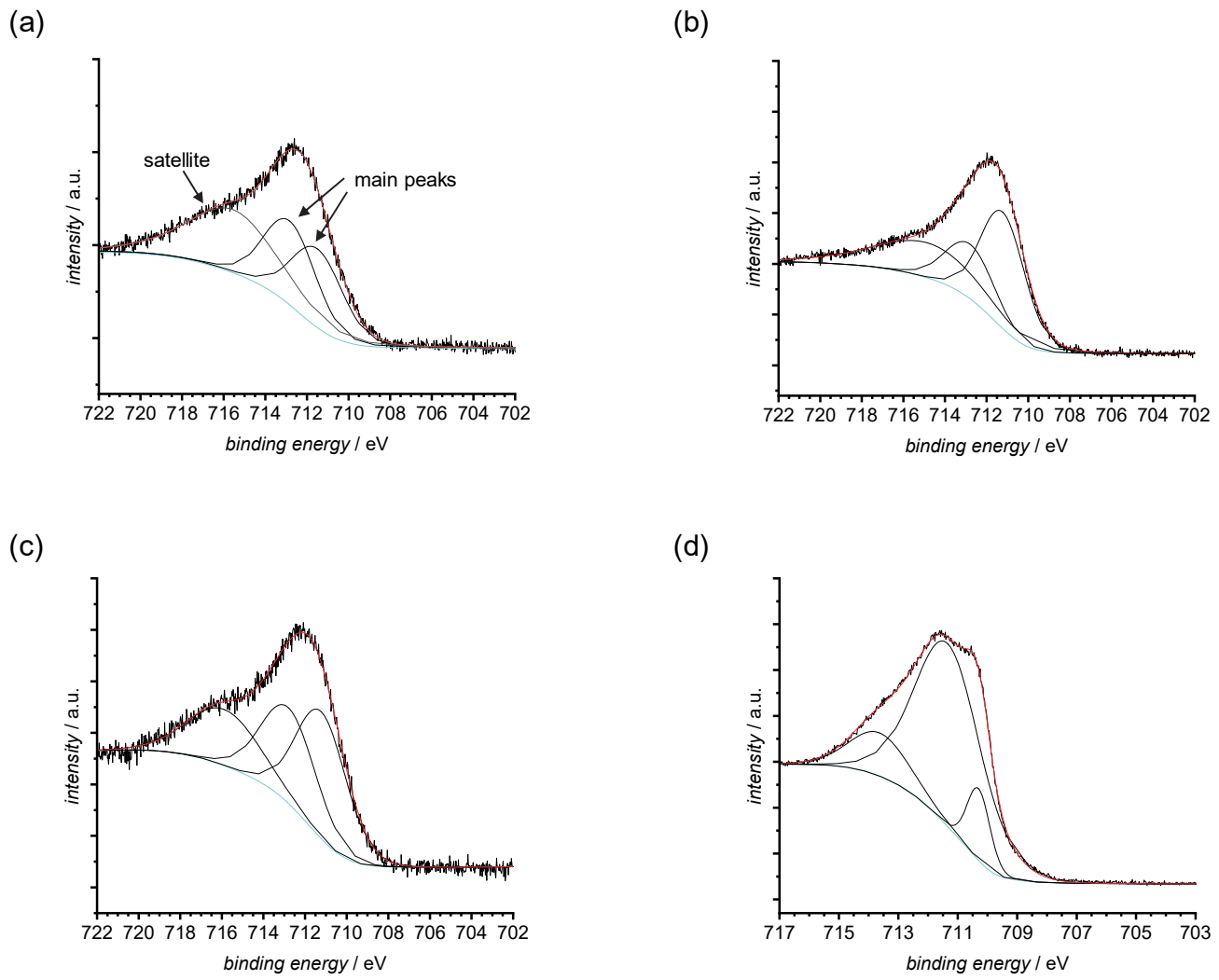


Fig. S11 XPS Fe 2p spectra for (a) MIL-53-lt, (b) NH<sub>2</sub>-MIL-88B, (c) MIL-88C and (d)  $\alpha$ -Fe<sub>2</sub>O<sub>3</sub>.

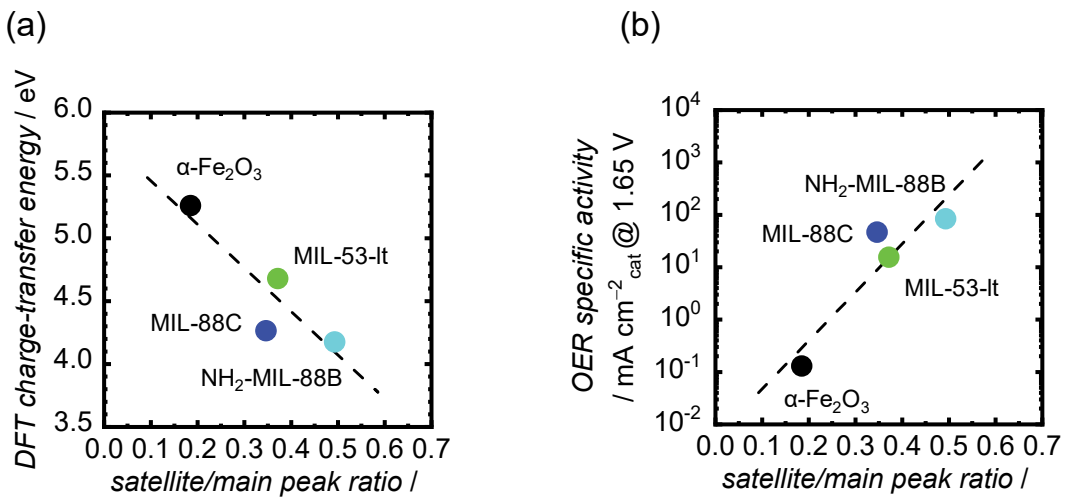


Fig. S12 (a and b) DFT-calculated charge-transfer energies and OER specific activities at 1.65 V, respectively, as a function of XPS-obtained satellite/main peak ratio in Fe 2p spectra.

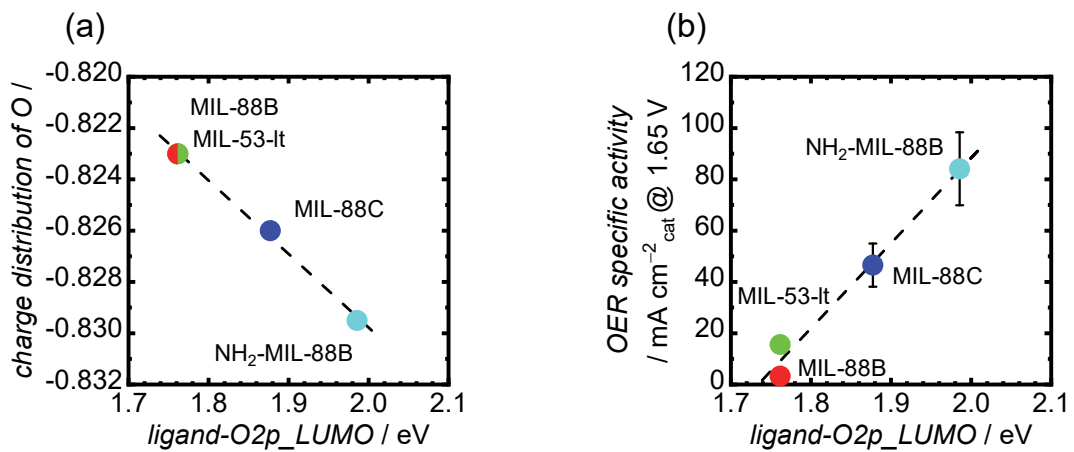


Fig. S13 (a) Relationships between the energy level of O<sub>2p</sub> LUMO of the organic ligand in each MOF

and the charge distribution on O in carboxylates in each organic ligand. (b) OER specific activities of the iron-based MOFs at 1.65 V as a function of the energy level of O<sub>2p</sub> LUMO of the organic ligands.

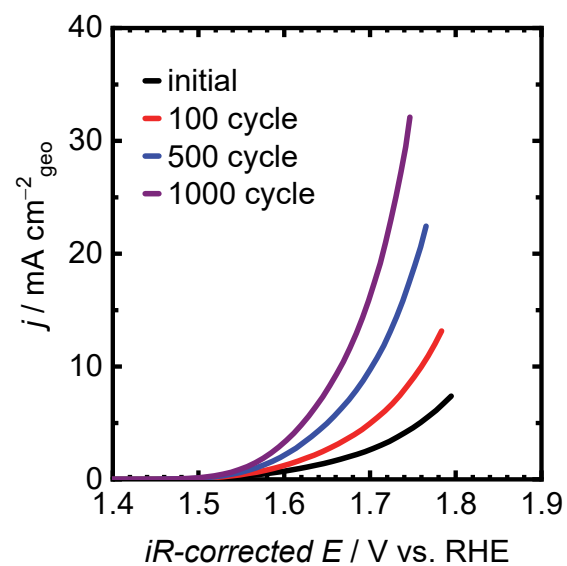


Fig. S14 OER polarization curves of  $\text{NH}_2\text{-MIL-88B}$  electrode before and after repeated potential cycles.

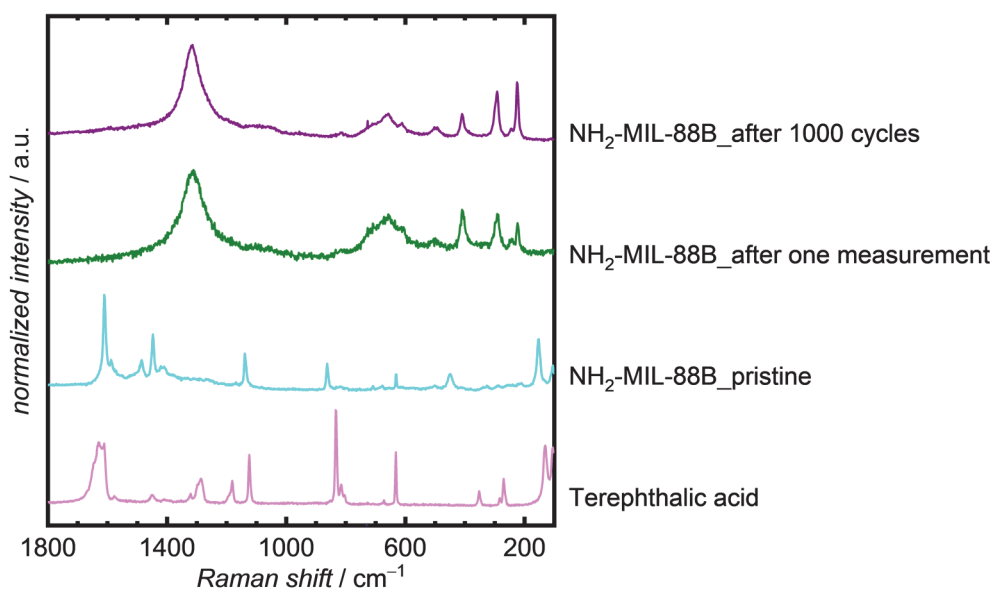


Fig. S15 Raman spectra of pristine and recovered NH<sub>2</sub>-MIL-88B after one OER measurement and 1000 potential cycles as well as terephthalic acid.

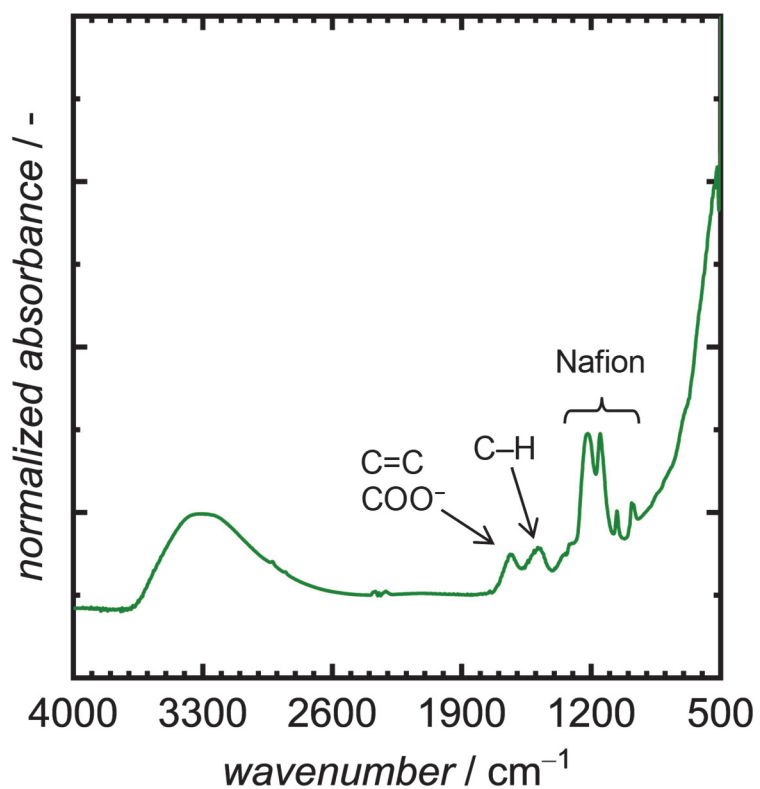


Fig. S16 FTIR spectrum of recovered NH<sub>2</sub>-MIL-88B after OER measurement.

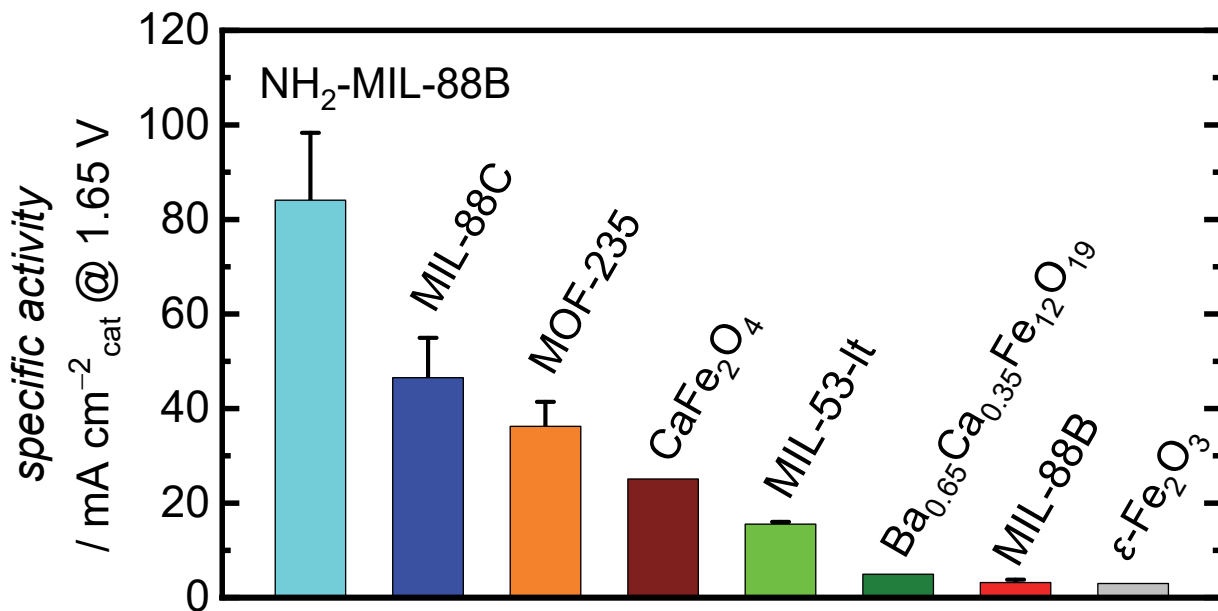


Fig. S17 Comparison of OER-specific activity at 1.65 V vs. RHE with previously reported iron-based oxides. The data for the iron-based oxides were adapted with permission from Ref. 12 Copyright 2021 American Chemical Society and permission from Ref. 17 and 18 Copyright 2021, 2022 John Wiley & Sons, Inc.

Table S1. The calculated unit cell sizes of the iron-based MOFs and Fe<sub>2</sub>O<sub>3</sub> polymorphs and k-points.

Catalyst	Lattice vector length <sup>a</sup> [Å]		<i>k</i> -point
MIL-88B	13.91050	13.91050	17.66080
MIL-53-lt	19.31970	15.03620	6.83510
NH <sub>2</sub> -MIL-88B	11.10750	11.10750	19.09250
MIL-88C	10.17510	10.17510	23.77220
			4×4×2

<sup>a</sup>Initial structures obtained experimentally and collected as CIF files from ICSD and CCDC cards.

Table S2. Electrochemical OER performance of the iron-based MOFs.

MOFs	Overpotential @0.5 mA cm <sup>-2</sup> <sub>cat</sub> <sup>a</sup> [V]	Tafel slope [mV dec <sup>-1</sup> ]	Specific activity @1.65 V <sup>b</sup> [mA cm <sup>-2</sup> <sub>cat</sub> ]
MIL-88B	0.35	170	3.2 ± 0.57
MOF-235	0.29	54	36 ± 5.2
MIL-53-lt	0.30	54	16 ± 0.44
NH <sub>2</sub> -MIL-88B	0.28	45	84 ± 14
MIL-88C	0.29	50	47 ± 8.4

<sup>a</sup>Obtained from OER polarization curves. <sup>b</sup>Calculated by measured currents in the OER polarization curves and specific surface areas.

Table S3. DFT-calculated O 2p and unoccupied Fe 3d band centers and charge-transfer energies for the iron-based MOFs, which were extracted from Fig. S10.

MOFs	Occupied O 2p band center [eV]	Unoccupied Fe 3d band center [eV]	Charge-transfer energy [eV]
MIL-88B	-3.13	2.13	5.25
MIL-53-lt	-2.33	2.35	4.68
NH <sub>2</sub> -MIL-88B	-1.97	2.21	4.18
MIL-88C	-1.64	2.62	4.26

Table S4. Peaks observed in the FTIR spectra of MOF-based electrocatalysts after OER measurements compared with literature values.

Starting MOF	Organic ligand	Wavenumber [cm <sup>-1</sup> ]	Ref.
NH <sub>2</sub> -MIL-88B (Fe)	2-Aminobenzene-	1630 (C=C, COO <sup>-</sup> ),	This study
	1,4-dicarboxylic acid	1489 (C-H)	
Ni-CAT	Hexahydroxytriphenylene	1610 (C=C), 1470 (C-H)	19
NiFeMn-MIL53	Terephthalic acid	1642 (COO <sup>-</sup> )	20
NiFeCP	Terephthalic acid	1630 (COO <sup>-</sup> ), 1400 (COO <sup>-</sup> )	21

Table S5. Comparison of OER-specific activity in 1 M KOH with the other previously reported MOF-based OER catalysts.

MOFs	Specific activity @1.60 V <sup>a</sup> [mA cm <sup>-2</sup> <sub>cat</sub> ]	Ref.
NH <sub>2</sub> -MIL-88B	27	This study
ZIF-FeCo MOF	2.3	22
Fe-NiNH <sub>2</sub> BDC/CNT	0.27	23
CoCd-BNN	0.13	24
IrFe-N-C	0.045	25
MAF-X27-OH(Cu)-2	0.018	26
Ti <sub>3</sub> C <sub>2</sub> Tx–CoBDC	0.0096	27
UTSA-16	0.0012	28

<sup>a</sup>Specific activity was calculated based on the current densities measured at 1.60 V vs. RHE, the catalyst loading amounts on each electrode and the specific surface areas of each MOF as reported in the referenced paper.

## Supporting Reference

1. M. A. Haydar, H. R. Abid, B. Sunderland and S. Wang, *Drug Des. Devel. Ther.*, 2017, **11**, 2685–2695.
2. R. Yuan, C. Yue, J. Qiu, F. Liu and A. Li, *Appl. Catal. B Environ.*, 2019, **251**, 229–239.
3. I. Simonsson, P. Gärdhagen, M. Andrén, P. L. Tam and Z. Abbas, *Dalton Trans.*, 2021, **50**, 4976–4985.
4. J. Liu, L. Fu, X. Peng, T. Pei, Z. Gao, W. Huang and Z. Zuo, *Chem. Lett.*, 2022, **51**, 99–102.
5. N. A. Ramsahye, T. K. Trung, L. Scott, F. Nouar, T. Devic, P. Horcajada, E. Magnier, O. David, C. Serre and P. Trems, *Chem. Mater.*, 2013, **25**, 479–488.
6. Y. G. Li, W. Zhou, H. L. Wang, L. M. Xie, Y. Y. Liang, F. Wei, J. C. Idrobo, S. J. Pennycook and H. J. Dai, *Nat. Nanotechnol.*, 2012, **7**, 394–400.
7. G. Kresse and J. Hafner, *Phys. Rev. B*, 1993, **47**, 558–561.
8. G. Kresse and J. Hafner, *Phys. Rev. B*, 1994, **49**, 14251–14269.
9. G. Kresse and J. Furthmuller, *Phys. Rev. B*, 1996, **54**, 11169–11186.
10. G. Kresse and J. Furthmuller, *Comput. Mater. Sci.*, 1996, **6**, 15–50.
11. J. P. Perdew, K. Burke and M. Ernzerhof, *Phys. Rev. Lett.*, 1996, **77**, 3865–3868.
12. Y. Sugawara, K. Kamata, A. Ishikawa, Y. Tateyama and T. Yamaguchi, *ACS Appl. Energy Mater.*, 2021, **4**, 3057–3066.
13. Gaussian 16 Revision C.01, M. J. Frisch, G. W. Trucks, H. B. Schlegel, G. E. Scuseria, M. A.

- Robb, J. R. Cheeseman, G. Scalmani, V. Barone, G. A. Petersson, H. Nakatsuji, X. Li, M. Caricato, A. V. Marenich, J. Bloino, B. G. Janesko, R. Gomperts, B. Mennucci, H. P. Hratchian, J. V. Ortiz, A. F. Izmaylov, J. L. Sonnenberg, D. Williams-Young, F. Ding, F. Lipparini, F. Egidi, J. Goings, B. Peng, A. Petrone, T. Henderson, D. Ranasinghe, V. G. Zakrzewski, J. Gao, N. Rega, G. Zheng, W. Liang, M. Hada, M. Ehara, K. Toyota, R. Fukuda, J. Hasegawa, M. Ishida, T. Nakajima, Y. Honda, O. Kitao, H. Nakai, T. Vreven, K. Throssell, J. J. A. Montgomery, J. E. Peralta, F. Ogliaro, M. J. Bearpark, J. J. Heyd, E. N. Brothers, K. N. Kudin, V. N. Staroverov, T. A. Keith, R. Kobayashi, J. Normand, K. Raghavachari, A. P. Rendell, J. C. Burant, S. S. Iyengar, J. Tomasi, M. Cossi, J. M. Millam, M. Klene, C. Adamo, R. Cammi, J. W. Ochterski, R. L. Martin, K. Morokuma, O. Farkas, J. B. Foresman and D. J. Fox, Gaussian, Inc., Wallingford CT, 2016.
14. A. V. Marenich, C. J. Cramer and D. G. Truhlar, *J. Phys. Chem. B*, 2009, **113**, 6378–6396.
15. G. K. Zhang, J. J. Pei, Y. S. Wang, G. W. Wang, Y. S. Wang, W. C. Liu, J. F. Xu, P. F. An, H. Huang, L. R. Zheng, S. Q. Chu, J. C. Dong and J. Zhang, *Angew. Chem. Int. Ed.*, 2024, **63**, e202407509.
15. A. C. Sudik, A. P. Côté and O. M. Yaghi, *Inorg. Chem.*, 2005, **44**, 2998–3000.
17. Y. Sugawara, K. Kamata, E. Hayashi, M. Itoh, Y. Hamasaki and T. Yamaguchi, *ChemElectroChem*, 2021, **8**, 4466–4471.
18. Y. Sugawara, S. Ueno, K. Kamata and T. Yamaguchi, *ChemElectroChem*, 2022, **9**, e202101679.

19. X. Wang, Z. Peng, W. Zhou, X. K. Chen, Y. Tan, Y. F. Huang, Z. Liu, W. Q. Deng and H. Wu, *Angew. Chem. Int. Ed.*, 2025, **64**, e202504148.
20. C. F. Li, J. W. Zhao, L. J. Xie, J. Q. Wu, Q. Ren, Y. Wang and G. R. Li, *Angew. Chem. Int. Ed.*, 2021, **60**, 18129–18137.
21. W. L. Li, F. S. Li, H. Yang, X. J. Wu, P. L. Zhang, Y. Shan and L. C. Sun, *Nat. Commun.*, 2019, **10**, 5074.
22. X. C. Gu, Y. G. Ji, J. Q. Tian, X. Wu and L. G. Feng, *Chem. Eng. J.*, 2022, **427**, 131576.
23. L. Yaqoob, T. Noor, N. Iqbal, H. Nasir, N. Zaman and K. Talha, *J. Alloy. Compd.*, 2021, **850**, 156583.
24. K. Maity, K. Bhunia, D. Pradhan and K. Biradha, *ACS Appl. Mater. Interfaces*, 2017, **9**, 37548–37553.
25. Z. P. Yu, C. W. Si, A. P. LaGrow, Z. X. Tai, W. A. Caliebe, A. Tayal, M. J. Sampaio, J. P. S. Sousa, I. Amorim, A. Araujo, L. J. Meng, J. L. Faria, J. Y. Xu, B. Li and L. F. Liu, *ACS Catal.*, 2022, **12**, 9397–9409.
26. X. F. Lu, P. Q. Liao, J. W. Wang, J. X. Wu, X. W. Chen, C. T. He, J. P. Zhang, G. R. Li and X. M. Chen, *J. Am. Chem. Soc.*, 2016, **138**, 8336–8339.
27. L. Zhao, B. L. Dong, S. Z. Li, L. J. Zhou, L. F. Lai, Z. W. Wang, S. L. Zhao, M. Han, K. Gao, M. Lu, X. J. Xie, B. Chen, Z. D. Liu, X. J. Wang, H. Zhang, H. Li, J. Q. Liu, H. Zhang, X. Huang and W. Huang, *ACS Nano*, 2017, **11**, 5800–5807.

28. J. Jiang, L. Huang, X. M. Liu and L. H. Ai, *ACS Appl. Mater. Interfaces*, 2017, **9**, 7193–7201.